



Sensitivity analysis of a 1 kW diesel-fuelled SOFC generator: A single and paired-variable study

Harsh Dhingra, Brant A. Peppley*

Queen's-RMC Fuel Cell Research Centre (FCRC), Queen's University, Kingston, ON K7L 5L9, Canada



HIGHLIGHTS

- A simulation of a 1 kW diesel-fuelled SOFC generator is developed.
- A sensitivity analysis is carried out to evaluate influence on system performance.
- Performance is most sensitive to changes in S/C ratio, fuel and air utilization.
- The interaction between fuel and air utilization is found to be an important one.
- Insight provided into tolerances of input variables with regards to performance.

ARTICLE INFO

Article history:

Received 21 August 2012

Received in revised form

11 March 2013

Accepted 14 March 2013

Available online 1 April 2013

Keywords:

Fuel-cell system

Diesel

SOFC

Autothermal reformer

Sensitivity analysis

ABSTRACT

Off-grid electricity generation creates a number of environmental, social and economic concerns for remote communities. This represents an opportunity for deployment of SOFC systems in remote areas for distributed power generation. In this paper, a simulation of a 1 kW diesel-fed SOFC system using an auto-thermal reformer is developed and studied using a sensitivity analysis. The influence of key design and operating variables on system performance, where system performance is characterized by the net system efficiency, gross stack efficiency and the final system exhaust temperature is examined. Selected paired variable sensitivities are also examined based on the ranking of individual sensitivities, where two variables at a time are adjusted simultaneously. Of the variables studied, it is observed that variability in the air utilization, fuel utilization and the steam to carbon ratio have the greatest impact on system performance. Overall, an insight is provided into the nature of operating variable interactions as well as those operating variables that require more rigorous process control. The work presented in this study is to be used as a tool by the SOFC Canada NSERC Strategic Network for the design and development of a demonstration small-scale diesel-fed SOFC system.

© 2013 Elsevier B.V. All rights reserved.

1. Introduction

According to Basu, Solid Oxide Fuel Cells (SOFCs) have been around since the end of the nineteenth century, when the basic ideas and materials for the technology were proposed by Nernst and his colleagues [1]. Baur and Pries, in 1937, were able to successfully operate a ceramic fuel cell at temperatures approaching 1000 °C [2]. Recent advancements, however, in producing thinner electrolytes and improved cathodes have reduced possible operating temperatures down to about 650 °C. The combination of fuel flexibility, the use of a solid electrolyte and high quality waste heat for cogeneration and potentially bottoming cycles make SOFCs an

attractive candidate for stationary residential or commercial applications, Auxiliary Power Units (APUs) for vehicles and also specialty military aircraft operations [3].

In fuel cells systems, the system configuration is often dictated by the choice of reforming scheme. Fuel reforming can occur via three possible routes, those being steam reforming (SR), auto-thermal reforming (ATR) and partial oxidation (POX). Sulphur tolerance typically increases from SR to POX, respectively, whereas hydrogen yield increases in the opposite direction. SR and POX both exhibit greater tendencies for carbon formation and therefore pose a greater risk for catalyst deactivation. Carbon formation is also more favoured for heavier fuels such as diesel and jet fuel due to the presence of higher molecular weight species and poorer mixing characteristics. An added advantage of the ATR fuel processor is that a smaller quantity of water is required compared to SR. This can be important for locations where a supply of clean water is

* Corresponding author. Tel.: +1 613 547 6700.

E-mail address: brant.peppley@queensu.ca (B.A. Peppley).

not present. An ATR can also provide thermo-neutral operation by controlling the relative amounts of air and fuel in the ATR feed [4,5].

There is environmental concern around the use of conventional diesel generators in many remote parts of Canada. In addition to producing unburned hydrocarbons, NO_x and particulate emissions, diesel engines generate noise and vibration and are also difficult to start in cold weather conditions. According to the National Energy Board of Canada (2011), there are an estimated 300 plus isolated communities that rely on diesel generators. Almost half of these communities are situated in the Northern Canada. In addition, the population sparsity of Northern Canada (just over 100,000 spread out over 3.5 million square kilometers) complicates the logistics and costs of energy distribution. Hydropower is the largest source of electricity in the North; however, the distribution is very limited. Nunavut, one of the three Northern provinces, is supported entirely by diesel generated electricity [6].

The cost of transporting diesel, the price of electricity generation in remote areas (in some Northern communities, electricity costs have been over 10 times the Canadian average on a per kilowatt-hour basis) and the extreme sensitivity of surrounding ecosystems provides motivation to replace the existing technology with SOFC systems [6]. Many of the existing generators in Northern Canada are built around communities. Diesel generators are known to generate a continuous background hum, whereas an SOFC power generation system would be considerably quieter. Furthermore, the introduction of SOFCs would significantly reduce the environmental impact of using heavy hydrocarbon fuels because of both reduced emissions and higher efficiency.

This paper presents a simulation of a small-scale 1 kW diesel-fed SOFC system using an ATR fuel processor under steady-state operation. In the current literature on diesel-fed SOFC systems, most use either steam reforming [7,8], CPOX [9,10] or TPOX [11] as part of their fuel processing methods, with ATR fuel processing directed primarily towards APUs [12–14]. The sensitivity of system performance in this paper is studied with respect to six design and operating variables. Three objective variables are chosen to characterize system performance, those being the net system efficiency, gross stack efficiency and the system exhaust temperature. Based on the assessment of the sensitivities, pairs of input variables are chosen for a second study to observe the nature of variable interactions around a set of base-line conditions. The simulation was developed in VMGSim™.

2. Process design

2.1. Diesel-fuelled SOFC process description

A schematic of the process modelled in VMGSim™ is depicted in Fig. 1, with an accompanying colour key for description of fluid streams. The Afterburner exhaust serves as the primary heating utility for the system. The need for energy from external sources can be avoided via thermal management in the system where heat recuperation is maximized and all other heating requirements are met by the Afterburner exhaust. The Afterburner exhaust is primarily used to heat the feed to the ATR. Additional waste heat, available from the SOFC anode and cathode exhaust streams, is used to pre-heat the air to the cathode to 800 °C and the incoming fuel to the liquid desulphurization temperature of 200 °C [15]. The SOFC unit operation in the simulation consists of a set of mass and energy balances in addition to a simplified electrochemical model. The zero-dimensional cell model used for the unit operation is obtained from an experimentally validated study conducted by Costamagna et al. [16] on a cathode-supported integrated-planar cell design. The cell model provides an estimate of the operating voltage of the stack as is expressed by the equations in Table 1.

Additionally, all the heat exchanger configurations are set to counter-current flow to allow for lower and relatively constant approach temperatures, with a hot stream inlet temperature being matched with the cold stream exit temperature. An arbitrary approach temperature of 30 °C is specified for heating the reactant mixture fed to the ATR. Lower approach temperatures when practical are desirable from a system efficiency standpoint in order to reduce entropy losses and maximizing efficiency [17]. The actual sizing of the heat-exchangers was not considered in the simulation.

In addition to the stream mixers and splitters, the remaining balance of plant (BoP) components include the air blower, the liquid adsorption desulphurization unit and the fuel and water pumps, all of which are represented as parasitic power losses in the system. The blower, which provided air at 1.07 bar, represented the largest parasitic power demand in the simulation. The parasitic losses were, however, small compared to the electrical energy produced by the stack.

2.2. Assumptions and approximations

The fuel composition chosen to represent the characteristics of the model diesel fuel is shown in Table 2. The mixture of hydrocarbons was developed such that the carbon to hydrogen ratio, level of aromatics and the boiling point curve was a close approximation to that of standard diesel fuel. Further assumptions and approximations are as follows:

- Negligible pressure drop throughout the system. The heat exchangers were, however, assigned minimal pressure drops on the order of 0.5–2 kPa.
- Negligible heat loss from the ATR and afterburner and thermo-neutral operation in the case of the ATR. The values of the associated energy streams, Q7 and Q8 are, therefore, zero. Both are modelled as Gibbs reactors, where the exit composition is determined from Gibbs free energy minimization.
- Homogeneous mixing of fuel, steam and air is achieved prior to the ATR.
- The desulphurization unit is a liquid adsorption separator [15] and the efficiency of sulphur removal is assumed to be 100%. Phenyl mercaptan is the only representative sulphur species present in the model diesel fuel in Table 2.
- CO does not oxidize in the fuel cell stack and the WGS reaction is assumed to be at equilibrium. The potential for CO undergoing direct oxidation at the anode is not significant. In addition, there is significantly more surface area at the triple-phase boundary for shift and reforming reactions than for oxidation [18]. In the simulation, CO is the limiting reactant in the WGS reaction for the anode stream entering the stack. To account for this in the simulation, CO is first reacted with steam to produce H₂ and CO₂ on a stoichiometric basis. In the last step of the simulation of the SOFC, the CO content of the anode exhaust is established based on the WGS equilibrium.
- The quantity of CH₄ entering the stack is negligible. There is no Direct Internal Reforming (DIR) of CH₄.
- Carbon formation is neglected.

2.3. Key definitions

The net system efficiency is defined as the net power output from the stack (after parasitic power is accounted for) over the lower heating value of the fuel entering the system (2.1). The parasitic losses are incurred from additional power requirements in the system such as the air compressor and are included as a penalty to η_{sys} .

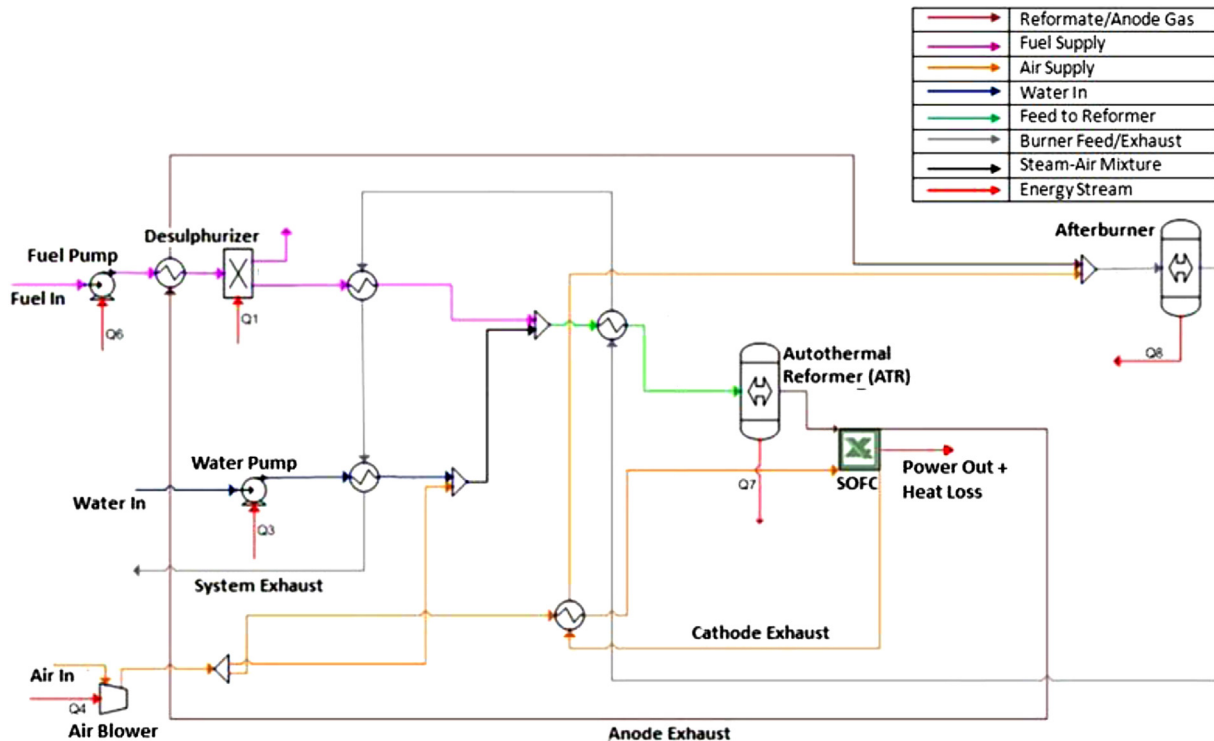


Fig. 1. Process flow diagram of 1 kW diesel-fed SOFC system.

$$\eta_{\text{SYS}} = \frac{W_{\text{elec}} - W_{\text{parasitic}}}{m_{\text{fuelin}} \text{LHV}_{\text{fuelin}}} \quad (2.1)$$

The gross stack efficiency is based on the ratio of the stack power output (not accounting for parasitic losses) and the LHV of the anode feed gas to the stack. The LHV is based on the CH₄, CO and H₂ content of the anode feed gas (2.2). CH₄, CO and H₂ are the only combustible species in the anode feed. The reformer efficiency (2.3) is similarly defined as the ratio of the LHV of the anode feed gas to the stack over the LHV of the fuel feed to the ATR. An approximate LHV of 42.5 MJ kg⁻¹ was used for (2.1) and (2.3) for the diesel composition presented in Table 1 [19].

$$\eta_{\text{SOFC}} = \frac{W_{\text{elec}}}{m_{\text{CO}} \text{LHV}_{\text{CO}} + m_{\text{CH}_4} \text{LHV}_{\text{CH}_4} + m_{\text{H}_2} \text{LHV}_{\text{H}_2}} \quad (2.2)$$

Table 1
SOFC zero-dimensional cell model equations[16].

Nernst equation	$V_{\text{Nernst}} = \frac{-\Delta G_f}{2F} + \frac{RT}{2F} \ln \left(\frac{p_{\text{H}_2} p_{\text{O}_2}^{0.5}}{p_{\text{H}_2\text{O}}} \right)$
Activation losses ^a	$V_{\text{act}} = \frac{2RT}{n_e F} \sinh^{-1} \left(\frac{i}{2i_0} \right)$ $i_{0,c} = \gamma_c \left(\frac{p_{\text{O}_2}}{P_{\text{ref}}} \right) \exp(-E_c/RT)$ $i_{0,a} = \gamma_a \left(\frac{p_{\text{H}_2}}{P_{\text{ref}}} \right) \left(\frac{p_{\text{H}_2\text{O}}}{P_{\text{ref}}} \right) \exp(-E_a/RT)$
Ohmic losses	$V_{\text{ohmic}} = iQ$
Concentration losses	$V_{\text{conc},a} = -\frac{RT}{n_e F} \ln \left(\frac{1 - (iRTt_a/n_e FD_{\text{eff},a} P X_{\text{H}_2})}{1 + (iRTt_a/n_e FD_{\text{eff},a} P X_{\text{H}_2})} \right)$ $V_{\text{conc},c} = -\frac{RT}{2n_e F} \ln \left(\frac{1}{X_{\text{O}_2}} - \left(\frac{1}{X_{\text{O}_2}} - 1 \right) \exp \left(\frac{iRTt_c}{2n_e FD_{\text{eff},c} P} \right) \right)$
Cell voltage	$V_{\text{Nernst}} - (V_{\text{act},a} + V_{\text{act},c}) - V_{\text{ohmic}} - (V_{\text{conc},a} + V_{\text{conc},c})$

^a Activation losses based on simplified Butler–Volmer expression where the charge transfer co-efficient is taken as 0.5 for both electrodes.

$$\eta_{\text{ATR}} = \frac{m_{\text{CO}} \text{LHV}_{\text{CO}} + m_{\text{CH}_4} \text{LHV}_{\text{CH}_4} + m_{\text{H}_2} \text{LHV}_{\text{H}_2}}{m_{\text{fuelin}} \text{LHV}_{\text{fuelin}}} \quad (2.3)$$

Fuel conversion is more challenging to quantify for higher hydrocarbon fuels such as diesel. There are variations in the literature and it is sometimes defined as the total conversion to gaseous carbon species such as CO, CO₂ and C₁–C₆ hydrocarbons as these compounds can be analyzed using a gas chromatograph or mass spectrometer. Equation (2.4) is, however, written in terms of molar flow rates of CO, CO₂, and CH₄ in the product as no significant C₂–C₆

Table 2
Diesel feed mixture molar composition.

n-Nonane	0.015998
n-Decane	8.90E-03
n-Undecane	4.60E-03
n-Dodecane	2.80E-03
n-Tridecane	1.40E-03
n-Tetradecane	1.50E-03
n-Pentadecane	3.30E-03
n-Hexadecane	0.006999
n-Heptadecane	0.014999
n-Octadecane	3.18E-02
n-Nonadecane	6.71E-02
n-Eicosane	0.138886
n-Pentylbenzene	8.37E-02
n-Hexylbenzene	6.03E-02
n-Heptylbenzene	4.88E-02
n-Octylbenzene	0.049995
n-Nonylbenzene	5.28E-02
n-Decylbenzene	5.12E-02
n-Undecylbenzene	0.118088
n-Dodecylbenzene	0.187781
Naphthalene	6.50E-03
1-Methylnaphthalene	3.30E-03
1-Ethynaphthalene	5.30E-03
1-Propynaphthalene	8.10E-03
1-n-Butynaphthalene	1.31E-02
Phenyl mercaptan	1.28E-02

hydrocarbons are produced in the simulation of the ATR that would influence system performance as characterized in the study. This form has also been reported in literature [5]. n_c in (2.4) is the weighted average number of carbon atoms per hydrocarbon molecule in the ATR feed.

$$\frac{n_{\text{CH}_4} + n_{\text{CO}} + n_{\text{CO}_2}}{n_c \times \text{Molar flow rate of hydrocarbons feed to ATR}} \quad (2.4)$$

The hydrogen yield in the ATR is defined as the molar flow rate of H₂ and CO in the product over the H₂ equivalent of the total molar flow rate of hydrocarbons fed to the reactor (2.5). The yield is defined as a function of H₂ and CO to include both H₂ production from reforming and any additional H₂ that is generated downstream by WGS. n_h represents the theoretical number of moles of hydrogen produced per mol of hydrocarbon [5].

$$\frac{n_{\text{H}_2} + n_{\text{CO}}}{n_h \times \text{Molar flow rate of hydrocarbons feed to ATR}} \quad (2.5)$$

Lastly, the fuel utilization in the stack is based on the hydrogen equivalent molar flow rate of H₂ and CO in the anode feed and anode exhaust to account for WGS [18]. (2.7) is expressed in terms of the total available molar flow rate of H₂ entering the stack. $\varepsilon_{\text{COMB}}$ represents the moles of H₂ consumed in the stack (2.6).

$$\varepsilon_{\text{COMB}} = \frac{i \times A \times n_{\text{cells}}}{2F} \quad (2.6)$$

$$U_f = \frac{\varepsilon_{\text{COMB}}}{(n_{\text{H}_2} + n_{\text{CO}})} \quad (2.7)$$

2.4. SOFC mass and energy balances

The SOFC mole balances are presented in Table 3. In the first column (CO shift), the total amount of CO entering the stack anode is converted to H₂ and CO₂ on a stoichiometric basis. This is based on the assumption listed in Section 2.2 (no direct oxidation of CO in the stack). The sum of the Initial and CO shift columns for the anode represents the anode feed to the stack. In the column denoted Electrochemical change, H₂ is consumed as current is drawn. Finally, WGS equilibrium is re-established by calculating the extent of the RWGS reaction, ε_{WGS} .

ε_{WGS} is determined by substituting the WGS equilibrium constant as a function of product and reactant flows (2.8) into a temperature dependent equilibrium constant expression (2.9) [20]. ε_{WGS} carries a negative value.

$$\ln(K_{\text{eq,WGS}}) = 4306.6/T_{\text{SOFC}} - 3.93 \quad (2.8)$$

$$K_{\text{WGS}} = \frac{((n_{\text{CO}_2} + n_{\text{CO}}) + \varepsilon_{\text{WGS}}) \left(\left(n_{\text{H}_2} + n_{\text{CO}} - \frac{i \times n_{\text{cells}}}{2F} \right) + \varepsilon_{\text{WGS}} \right)}{(-\varepsilon_{\text{WGS}}) \left(\left(n_{\text{H}_2} - n_{\text{CO}} + \frac{i \times n_{\text{cells}}}{2F} \right) - \varepsilon_{\text{WGS}} \right)} \quad (2.9)$$

The SOFC energy balance (2.10) consists of enthalpy terms in and out of the stack, the heat of reaction for the electrochemical combustion of the fuel (2.12) and WGS, an electrical power output and a heat loss term. The input and output enthalpies are calculated from (2.11).

$$\sum_{i=1}^k H_i^{\text{in}} - \sum_{i=1}^k H_i^{\text{out}} - Q_{\text{rxn}} = W_{\text{elec}} + Q_{\text{loss}} \quad (2.10)$$

$$H_i = m_i C_{\text{pi}} (T_i - T_{\text{ref}}) \quad (2.11)$$

$$Q_{\text{rxn}} = \varepsilon_{\text{COMB}} \Delta H_{\text{COMB}}^0 + (n_{\text{CO}} + \varepsilon_{\text{WGS}}) \Delta H_{\text{WGS}}^0 \quad (2.12)$$

The total heat loss in the stack Q_{loss} was set to an arbitrary value of 400 W in the simulation.

2.4.1. Process simulation controllers

In the setup of the mass and energy balances, a subroutine in VMGSim is used that calculates the stack temperature. The subroutine is performed using a controller operation. The output temperature of the stack, T_{SOFC} is adjusted until the energy balance is satisfied. The target value is thus the RHS of (2.10), or the sum of the electrical power output from the stack and the heat loss. The stack power is, however, a variable, with a direct dependency on the applied current and voltage. The controller set point is, therefore, also a variable quantity in the controller as seen in Table 4. A total of two controllers are applied in the simulation in addition to a recycle stream required for the anode stream to the stack. An initial guess is required for the recycle stream for convergence to be achieved. The controller parameters are summarized in Table 3. MV, SP, and TV are acronyms for the manipulated variable, set point and target variable, respectively.

3. Results

The significance of various process operating and design variables was assessed as a function of the performance metrics

Table 3
SOFC mol balance.

Anode	Initial	CO shift	Electrochemical change	Re-establish WGS equilibrium	Final (anode exhaust)
CO	n_{CO}	$-n_{\text{CO}}$	—	$-\varepsilon_{\text{WGS}}$	$-\varepsilon_{\text{WGS}}$
H ₂	n_{H_2}	n_{CO}	$-\frac{i \times A \times n_{\text{cells}}}{2F}$	ε_{WGS}	$n_{\text{H}_2} + n_{\text{CO}} - \frac{i \times A \times n_{\text{cells}}}{2F} + \varepsilon_{\text{WGS}}$
H ₂ O	$n_{\text{H}_2\text{O}}$	$-n_{\text{CO}}$	$\frac{i \times A \times n_{\text{cells}}}{2F}$	$-\varepsilon_{\text{WGS}}$	$n_{\text{H}_2\text{O}} - n_{\text{CO}} + \frac{i \times A \times n_{\text{cells}}}{2F} - \varepsilon_{\text{WGS}}$
CO ₂	n_{CO_2}	n_{CO}	—	ε_{WGS}	$n_{\text{CO}_2} + n_{\text{CO}} + \varepsilon_{\text{WGS}}$
CH ₄	n_{CH_4}	—	—	—	n_{CH_4}
N ₂	n_{N_2}	—	—	—	n_{N_2}
Cathode	Initial		Electrochemical change		Final (cathode exhaust)
O ₂		n_{CO}	$-\frac{i \times A \times n_{\text{cells}}}{4F}$		$n_{\text{O}_2} - \frac{i \times A \times n_{\text{cells}}}{4F}$
N ₂		n_{CO}	—		n_{N_2}

Table 4

Controller inputs and outputs.

Controller	MV	SP	TV
Fuel utilization	m_{fuelin}	Constant	U_f
Energy balance	T_{SOFC}	$W_{\text{elec}} + Q_{\text{loss}}$	$\sum_{i=1}^k H_i^{\text{in}} - \sum_{i=1}^k H_i^{\text{out}} - \varepsilon_{\text{COMB}} \Delta H_{\text{COMB}}^0 - (n_{\text{CO}} + n_{\text{WGS}}) \Delta H_{\text{WGS}}^0$

described earlier in the chapter. The base-case cell settings and the list of applied constraints for the simulation (sensitivity analysis and paired-variable study presented in the next section) are presented in Tables 5 and 6, respectively. The operating and design variables of interest, assessed in the study, are depicted below.

- Air utilization (U_a) in the stack
- Fuel utilization (U_f) in the stack
- Oxygen to carbon (O_2 to C) ratio in feed to ATR
- Steam to carbon (S/C) ratio in feed to ATR
- Inlet cathode temperature to stack
- Pre-heater approach temperature to ATR

The effect of independent variables on system performance was studied for a constant current density and within the constraints defined in Table 6. All other conditions were kept at the baseline values in Table 5 while an independent variable was varied. The baseline efficiencies were 37% (net system) and 40% (gross stack). The baseline system exhaust temperature was 217 °C. The baseline conditions and model constraints were chosen based on the cell model [16] and from the range of values reported in various textbooks [18,19,21].

3.1. One at a time sensitivity analysis

3.1.1. Effect of air utilization

The effect of an increase in U_a in the SOFC (or a decrease in the feed air flow rate) for a fixed current density, is an increase in the net system efficiency and gross stack efficiency (Fig. 2). This is in part attributed to the lower power requirements of the air blower as a lower air flow rate to the system was supplied. Secondly, a smaller air flow rate to the stack results in less air available for stack cooling and gives rise to an increase in the stack temperature. Operation at higher stack temperatures in the simulation reduces both ohmic and activation losses and contributes to an increase in the stack voltage. High stack temperatures can also contribute to material degradation over time resulting in voltage losses. As the simulation was carried out at steady-state, the influence of material

degradation over time on stack performance was not considered. Thirdly, an increase in the stack temperature also results in an increase in the burner exhaust temperature throughout the studied U_a range. For a constant ATR pre-heater approach temperature, the temperature of the feed to the ATR is increased, giving rise to a greater hydrogen yield (the production of methane is also reduced with the rise in the temperature of the ATR). A smaller system fuel feed rate is, therefore, required for a constant current density and fuel utilization. The reduced air flow to the stack also reduces the partial pressure of O_2 in the stack and would eventually result in a decrease in the net system efficiency and gross stack efficiency. The combined effects of lower air blower power requirements, a higher stack temperature and a greater hydrogen yield in the ATR are, however, more dominant over the range of U_a 's tested. The variation in the stack temperature and the log mean O_2 partial pressure in the SOFC cathode with air utilization are shown in Fig. 3.

An increase in the burner exhaust temperature initially results in a higher system exhaust temperature as seen in Fig. 2 above. Beyond a utilization factor of approximately 20%, however, a decrease in the system exhaust temperature is observed. This observed effect is attributed to a reduction in the total mass flow rate of the burner exhaust stream with increasing U_a , and to unused air comprising of a large mass fraction of the exhaust. The energy content of the burner exhaust stream is, therefore, reduced and results in a lower system exhaust temperature.

3.1.2. Effect of fuel utilization

The effect of U_f was studied over the range from 50 to 90%. A reduction in the fuel feed rate results in a decrease in the average partial pressure of hydrogen in the stack as a consequence of the increased U_f . A decrease in stack power output is, therefore, observed. Both net system efficiency and gross stack efficiency gains are, however, observed over the simulation range (as seen in Fig. 4) as there is a greater reduction in the total LHV of the fuel feed ($m_{\text{fuelin}} \text{LHV}_{\text{fuelin}}$).

Less pre-heated steam is required with increasing U_f for a constant S/C ratio; however, a smaller fuel feed rate to the system results in less fuel to the burner. A lower system exhaust temperature is consequently observed.

Table 5

Base-case system settings.

System settings			
Thermodynamic model	Lee–Kesler	SOFC pressure	1.04 atm
S/C	3	Stack outlet temperature	865 °C
O_2 to C	0.25	SOFC cell voltage	0.693 V
Fuel utilization	80%	Cathode inlet temperature	800 °C
Air utilization	25%	ATR pre-heater approach temperature	30 °C
Stack power	1023 W	ATR fuel conversion	100%
Cell settings			
Cell current	15 A	Anode thickness	20 μm
Cell area	100 cm ²	Cathode thickness	500 μm
Number of cells	98	Electrolyte thickness	20 μm
Cell pitch length	1 cm	Interconnect thickness	500 μm ^a

^a Ref. [25].**Table 6**

Model constraints.

Variable	Min	Max
Stack power output	0.8 kW	1.2 kW
Average stack temperature	—	≤1000 °C
Average ATR temperature	500 °C	1000 °C
ATR fuel conversion	≥99%	—
ATR efficiency	≥80%	—
ATR hydrogen yield (based on H ₂ and CO product)	≥100%	—
Cathode exhaust post-recuperator temperature to burner	≥30 °C	—
Minimum heat-exchanger approach temperature	10 °C	—
Cathode temperature to stack	500 °C	840 °C
O_2 to C ratio	0.15	0.5
S/C ratio	2	4.5
ATR pre-heater heat-exchanger approach temperature	10 °C	200 °C
Fuel utilization	50%	90%
Air utilization	15%	50%

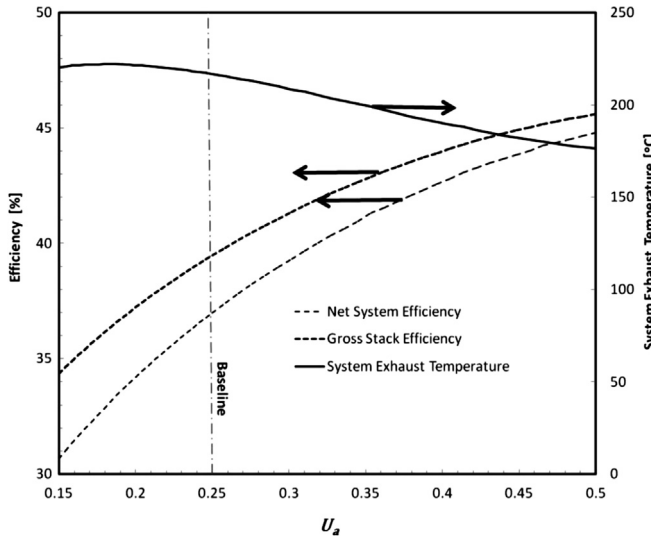


Fig. 2. Effect of air utilization on objective variables.

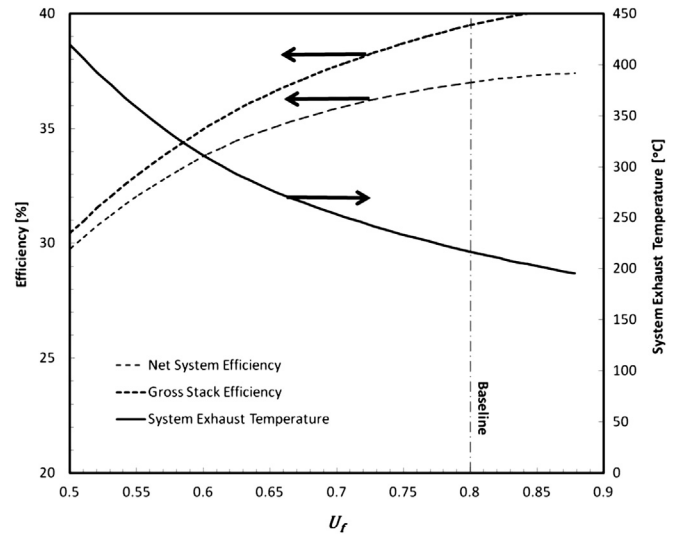


Fig. 4. Effect of fuel utilization on objective variables.

3.1.3. Effect of O₂ to C ratio

In the process diagram in Fig. 1, air at 20 °C is mixed with superheated steam followed by mixing with vaporized diesel fuel. The resulting mixture is pre-heated to a temperature based on the heat exchanger approach temperature prior to entering the ATR.

The net system efficiency and gross stack efficiency are initially observed to rise with increasing O₂ to C ratio (Fig. 5). Additional air entering the ATR increases the hydrogen yield and therefore lowers the fuel feed requirements for the system. The increase in hydrogen yield is attributed to the exothermic heat of combustion serving as a heat source for the endothermic steam reforming of diesel to hydrogen.

An O₂ to C ratio greater than approximately 0.35, however, has a negative effect on efficiency. A lower hydrogen yield in the ATR is observed due to excess fuel oxidation, in addition to the unfavourable change in the WGS equilibrium (formation of H₂O and CO from CO₂ and H₂) at higher temperatures (in the ATR as well as in the stack). The fuel feed requirements for the system are thus raised, resulting in lower efficiencies.

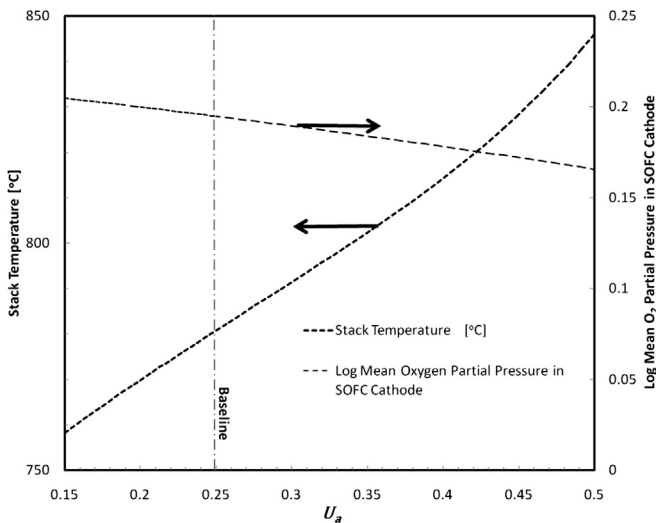


Fig. 3. Effect of air utilization on stack temperature and log mean O₂ partial pressure in SOFC cathode.

In comparison to the net system efficiency and gross stack efficiency, an increase in the O₂ to C ratio results initially in a decrease followed by an increase in the system exhaust temperature as shown in Fig. 5. The initial decrease in the system exhaust temperature is due to the additional pre-heating of the mixed air, steam and fuel stream entering the ATR. Furthermore, there is a heat capacity effect as the mass flow rates of H₂O and CO₂ in the burner exhaust are initially lowered as the O₂ to C ratio to the ATR is increased (Fig. 6) (H₂O in the burner exhaust has the highest specific heat capacity on a mass basis). The reduction in these mass flow rates is attributed to an increase in hydrogen production from steam reforming in the ATR as well as the change in the WGS equilibrium in the stack at higher stack temperatures (reducing the flow of CO₂ out of the stack). The reduction in the fuel feed rate to the system in this initial region with increasing O₂ to C ratio also reduces the amount of H₂O required in the ATR for a constant S/C ratio. The overall effect is a decrease in the heat capacity, energy content and the temperature of the burner exhaust stream and also a decrease in the system exhaust temperature.

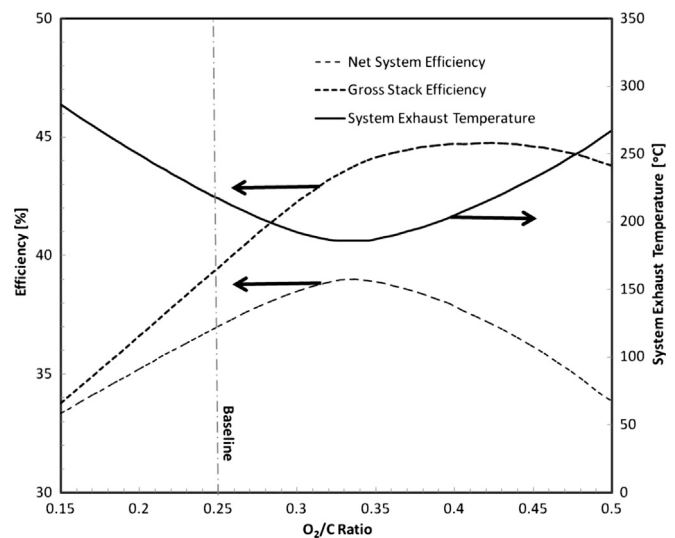


Fig. 5. Effect of O₂ to C ratio on objective variables.

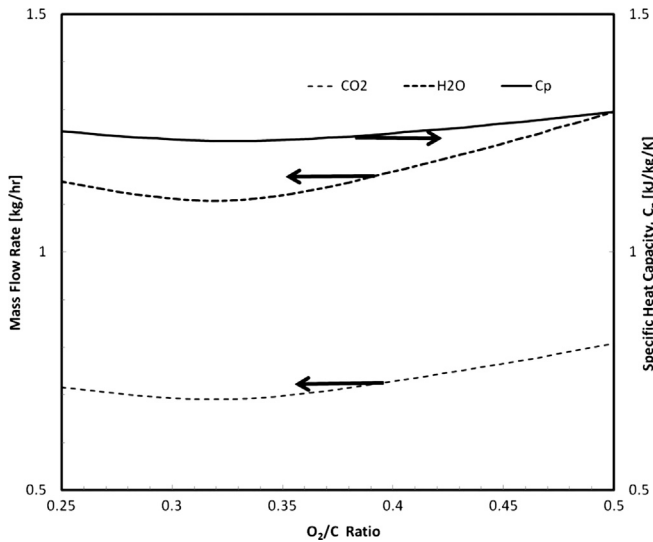


Fig. 6. Effect of O₂ to C ratio on CO₂ and H₂O molar flow rates in burner exhaust.

The system exhaust temperature begins to rise as the O₂ to C ratio is increased past approximately 0.35. The increase in the system exhaust temperature is in part attributed to the increase in the flow rate of the burner exhaust associated with the additional CO₂ and H₂O produced by fuel oxidation in the ATR. In addition, there is an increase in the stream's heat capacity and is as a result of the increased concentrations of H₂O and CO₂.

3.1.4. Effect of steam to carbon ratio

The molar flow rate of water entering the system is determined by the specified S/C ratio based on the weighted average number of carbon atoms per molecule in the diesel fuel feed. An increase in the S/C ratio is initially accompanied by a slow rise in the net system efficiency and gross stack efficiency as the hydrogen yield in the ATR is increased (Fig. 7).

An increase in the hydrogen yield reduces the fuel flow requirements to the system and, therefore, the total heating value of the feed stream. As more steam is added, however (an S/C > ~2.5), the H₂ downstream in the stack becomes increasingly diluted, resulting in a lower H₂ partial pressure [13]. A lowering of the stack

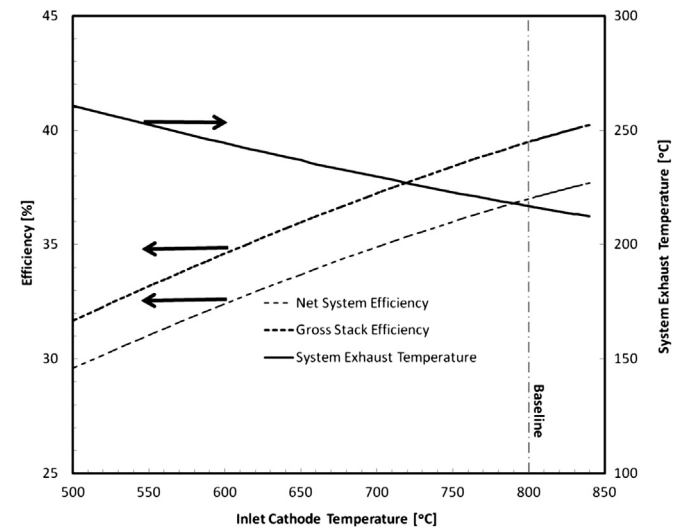


Fig. 8. Effect of inlet cathode temperature to SOFC on objective variables.

power output is, therefore, observed. Secondly, the increase in the hydrogen yield is less pronounced with an increasing amount of steam and the overall effect is a loss in net system efficiency and gross stack efficiency.

Lastly, the system exhaust temperature as can be seen in Fig. 7, decreases with an increasing S/C ratio. This is attributed to the following. Firstly, being a lower stack temperature and the temperature of the anode and cathode exhaust streams exiting the stack and entering the burner are lower. Secondly, additional pre-heating of the ATR feed is required with more steam entering the system at higher S/C ratios. Additional pre-heating is also required to provide the latent heat of vaporization for generating steam.

3.1.5. Effect of inlet cathode temperature to stack

The simulation predicts an increase in efficiency as the temperature of the cathode stream to the stack increases, as seen in Fig. 8. The higher temperature cathode feed stream increases the temperature of the stack and this results in an increase in the stack voltage and power output. The increase in stack power contributes

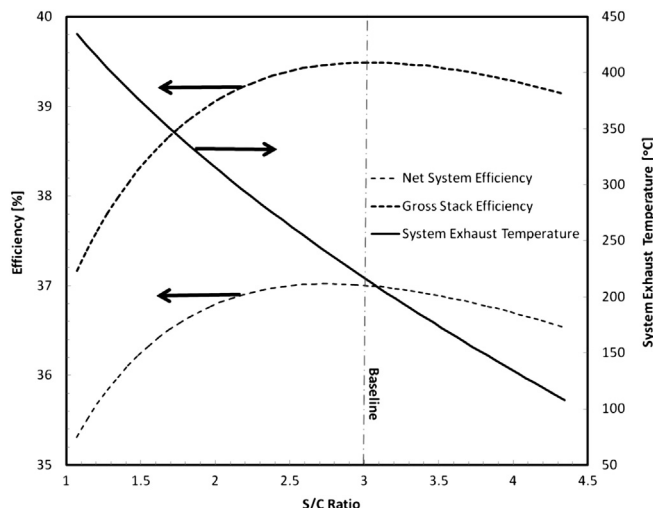


Fig. 7. Effect of S/C ratio on objective variables.

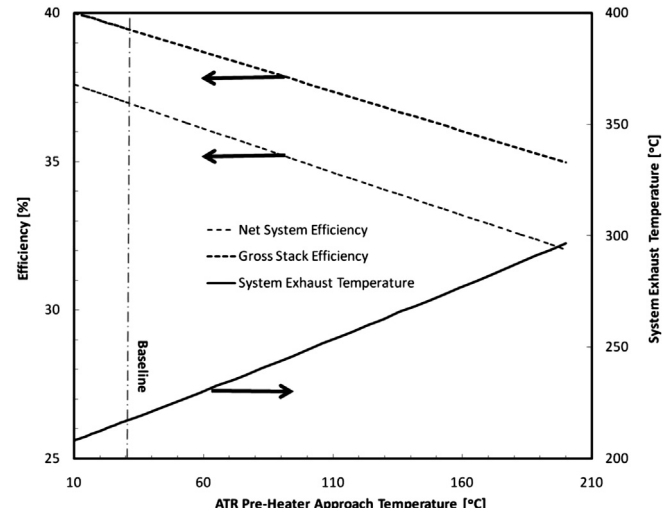


Fig. 9. Effect of ATR pre-heater approach temperature.

Table 7
Assessment of sensitivities.

Performance measure	Method 1	Method 2
System exhaust temperature	S/C ratio, U_f , O ₂ to C ratio	O ₂ to C ratio, U_f , U_a
Net system efficiency	U_a , cathode inlet temperature, U_f	U_a , O ₂ to C ratio, U_f
Gross stack efficiency	U_a , U_f , O ₂ to C ratio	O ₂ to C ratio, U_a , U_f

to the rise in the net system efficiency and gross stack efficiency. A higher inlet temperature to the SOFC cathode also results in a lower cathode exhaust post-recuperator temperature to the burner and a lower system exhaust temperature as seen in Fig. 8.

3.1.6. Effect of ATR pre-heater approach temperature

The lower the approach temperature (or the larger the heat-transfer surface area in the heat-exchanger) in the ATR pre-heater, the more effective is the heat-exchange. A lower approach temperature in the heat-exchanger results in an increase in the temperature of the ATR feed (Fig. 9). This means a smaller feed fuel flow rate is required to maintain the set fuel utilization with a greater hydrogen concentration at the ATR exit. An increase in stack power is also observed with a rise in the stack temperature. The overall effect is once again an increase in the net system efficiency and gross stack efficiency. The system exhaust temperature decreases in a linear fashion with a lower approach temperature as pre-heating requirements are raised, which would be expected as more heat is recovered from the burner exhaust.

Higher approach temperatures also significantly influences the hydrogen yield and; therefore, a maximum approach temperature of approximately 200 °C was used in the simulation case-study, based on the constraints listed in Table 6. Thus, a highly integrated heat-exchanger setup is important from a design standpoint in order to achieve high net system efficiency and gross stack efficiency. Furthermore, the steam reforming reaction is favourable at

lower approach temperatures and a lower O₂ to C ratio can be used to produce the same amount of hydrogen.

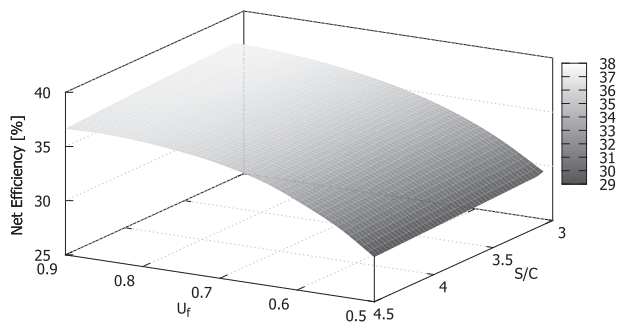
3.2. Paired-variable sensitivity analysis

3.2.1. Sensitivity ranking of variables

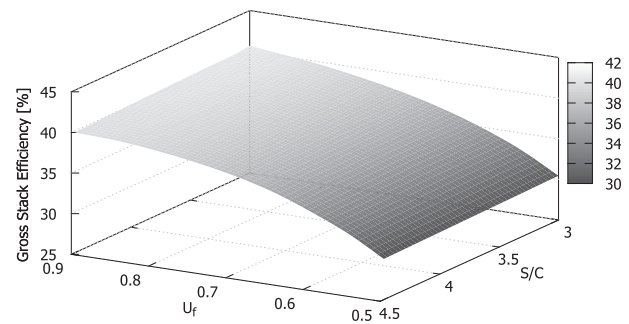
The sensitivity of predicted system performance with respect to changes in the independent variables was quantitatively assessed to produce a sensitivity ranking. The sensitivity ranking was determined using two different methods and is presented in Table 7. In the first case, a Sensitivity Index (SI) was calculated based on finding the difference in the maximum and minimum output value (of the system performance variable) when evaluating one input variable over its entire simulation range [22,23] and is expressed by (3.1). D represents the output value of the performance metric (Method 1). In Method 2, localized sensitivities were determined by varying input variables one at a time by 5% above and below their base case values and determining the corresponding ratio of the difference in input and output. According to Hamby (1994) [22,23], for a moderate number of independent variables, the SI is the easiest and most reliable sensitivity measure as it can be calculated without detailed knowledge about the variable and without the use of random sampling techniques. For each method in Table 7, the top three ranked independent variables are presented in order of decreasing sensitivity.

$$\frac{D_{\max} - D_{\min}}{D_{\max}} \quad (3.1)$$

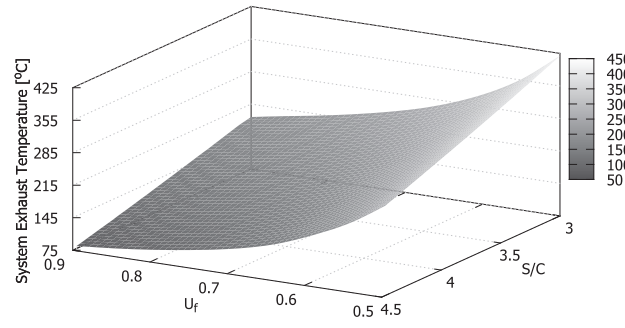
A repeated occurrence of top ranked independent variables is observed in the rankings obtained from both methods. The system exhaust temperature is found to be the most sensitive to changes in the S/C ratio, O₂ to C ratio and U_f . On the other hand, the net system efficiency and gross stack efficiency are most sensitive to changes in the O₂ to C ratio, U_a and U_f .



(a) Net System Efficiency



(b) Gross Stack Efficiency



(c) Exhaust Temperature

Fig. 10. U_f –S/C ratio interaction effects; (a) net system efficiency (b) gross stack efficiency (c) exhaust temperature.

3.2.2. Sensitivity analysis

In order to better understand the behaviour of the system around the base-case settings, two pairs of independent variables were chosen from Table 7. A paired-variable study was then carried out based on the constraints from Table 6 and for a constant current density. In one case, U_f and U_a were varied simultaneously to determine the highest net system efficiency and gross stack efficiency among the data collected. Similarly, U_f and S/C ratio were varied to obtain the lowest system exhaust temperature among the data collected. The two cases were plotted in the three-dimensional surface plots in Figs. 10 and 11, based on a total of 258 and 232 simulation results, respectively. Table 8 lists the domains used for the independent variables (U_f , U_a and S/C ratio).

The interactions observed in five of the six surface plots are the same as the original sensitivity analysis where the independent variables were varied one at a time. The exception to this is the observed relationship between U_f , U_a and the system exhaust temperature. In Fig. 11, at lower values of U_f and for a fixed current density, additional fuel enters the burner and results in an increased burner exhaust temperature. Secondly, at lower U_f values, the result of a large increase in the stack temperature with an increasing U_a is an increase in the system exhaust temperature. The result is different from what is observed over the majority of the base-case sensitivity analysis (at a fixed U_f ; 80%), where the system exhaust temperature decreases with an increasing U_a . The trend is shown again in Fig. 12 for clarity. The stack temperature was constrained to <1000 °C in the analysis and, therefore, not all points

Table 8
Independent variable simulation ranges.

Independent variable	Minimum	Maximum
U_f	0.5 (50%)	0.9 (90%)
U_a	0.25 (25%)	0.5 (50%)
S/C ratio	3	4.5

over the U_a range (25–50%) are included in the figures. Knowledge about the range of the operating variables beyond which stack overheating occurs is important when designing process control strategies for SOFC systems.

The constrained optimum values of the performance metrics over the simulation range as determined from the surface plots and based on the constraints in Table 6 are listed in Table 9. The lowest exhaust temperature is observed at a high U_f and S/C ratio. The highest net system efficiency and gross stack efficiency are observed at a high U_f and also a high U_a . The net efficiencies observed lie within the range of efficiencies reported by Delphi for their small-scale APU systems using CPOX reformers [24]. Baratto et al. [12] have also reported net efficiencies close to 40% in their simulation of a 5 kW diesel-fuelled SOFC APU with an ATR fuel processor.

It should be noted that this analysis has focused on the three highest ranked operating variables in terms of system performance sensitivity. To obtain the global optimum of the system performance, all design variables would need to be considered.

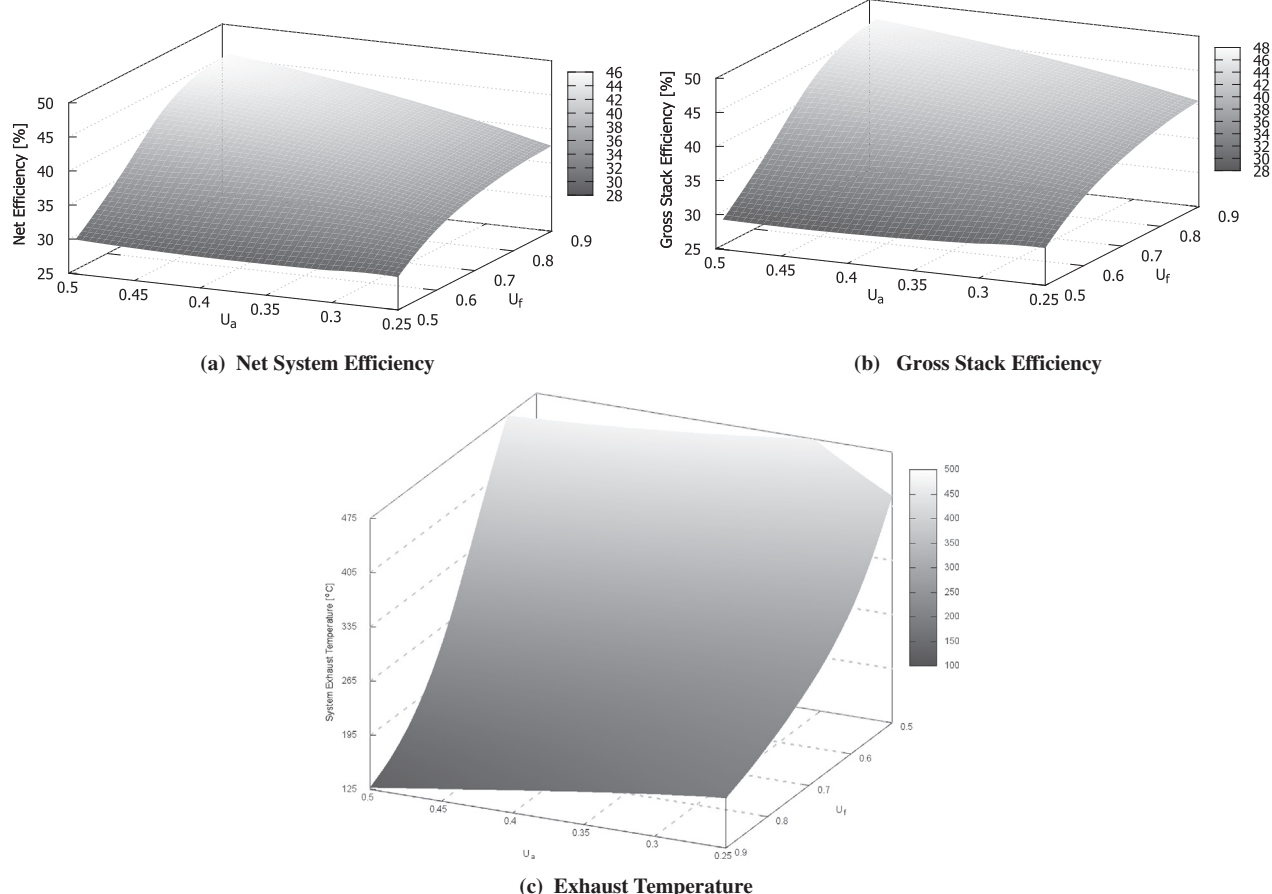


Fig. 11. U_f – U_a interaction effects; (a) net system efficiency (b) gross stack efficiency (c) exhaust temperature.

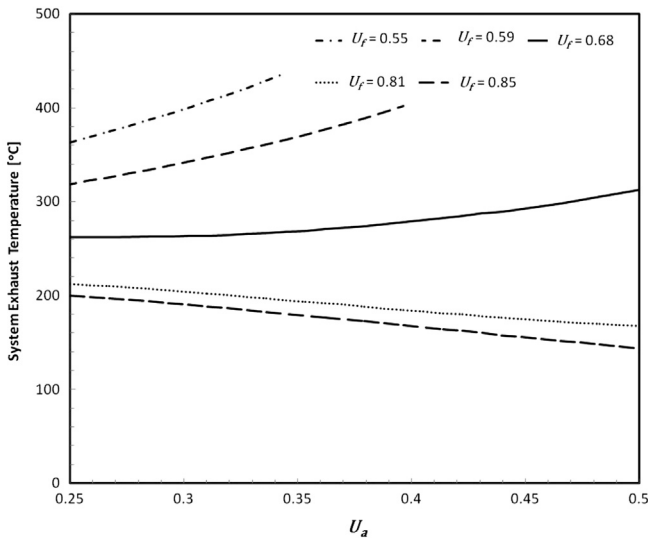


Fig. 12. U_f – U_a : influence on system exhaust temperature.

Table 9
Optimum values of objective variables over the simulation range.

	Net system efficiency [%]	Gross stack efficiency [%]	System exhaust temperature [°C]
Net system efficiency and gross stack efficiency maximum ^a	45	47	128
Lowest exhaust temperature ^b	37	40	78

^a $U_f = 0.9$, $U_a = 0.5$, S/C = 3.

^b $U_a = 0.25$, $U_f = 0.9$, S/C = 4.5.

4. Conclusion

A simulation of a 1 kW diesel-fuelled SOFC system was developed and a sensitivity analysis was carried out to investigate the influence of key design and operating variables and their influence on system performance.

- The gross stack efficiency and net system efficiency were observed to be most sensitive to the fuel (reformate) and air utilization in the stack. The system exhaust temperature, on the other hand, was most sensitive to the S/C ratio, because a greater heat of vaporization was required at higher ratios to generate steam.
- A paired-variable analysis revealed a difference in system behaviour that was not observed in the individual sensitivity analysis. It was found that, at lower fuel utilizations, higher air utilization factors were not desirable. The limitation in the air utilization factor at low fuel utilizations was attributed to the significant increase in the stack temperature from additional fuel entering the burner as well as less excess air available for stack cooling.
- A maximum net system efficiency and gross stack efficiency of 45% and 47%, respectively, were observed at $U_f = 0.9$, $U_a = 0.5$ and S/C = 3. A minimum system exhaust temperature of 78 °C was achieved for $U_a = 0.25$, $U_f = 0.9$ and S/C = 4.5.

The sensitivity analysis provided insights into what to expect with regards to system performance and stack temperature should

one or more of the independent variables deviate from their steady state values during process operation. The uncertainty in these values dictates how reliably the lower and upper bounds of system performance as dictated by the control scheme can be met as well as where more rigorous process control strategies may be desirable.

Acknowledgements

This work was funded and supported by the SOFC Canada NSERC Strategic Network. We would also like to acknowledge Adam Tuck from the National Research Council (NRC) in Vancouver, Canada for his valuable inputs in the project.

Nomenclature

A	cell area, m^2
C	heat capacity, $\text{kJ kg}^{-1} \text{K}^{-1}$
D	diffusion coefficient, $\text{m}^2 \text{s}^{-1}$
E	activation energy, kJ mol^{-1}
F	Faraday constant, C mol^{-1}
H	enthalpy, kJ kmol^{-1}
i	current density, A m^{-2}
i_0	exchange current density, A m^{-2}
K_{eq}	equilibrium constant
LHV_{CO}	lower heating value CO at anode feed, kJ kg^{-1}
LHV_{CO_2}	lower heating value CO_2 at anode feed, kJ kg^{-1}
LHV_{CH_4}	lower heating value CH_4 at anode feed, kJ kg^{-1}
LHV_{fuelin}	lower heating value fuel feed to SOFC system, kJ kg^{-1}
$LHV_{\text{fueltoref}}$	lower heating value fuel feed to reformer, kJ kg^{-1}
m_{fuelin}	mass flow rate fuel feed to SOFC system, kg s^{-1}
$m_{\text{fueltoref}}$	mass flow rate fuel feed to reformer, kg s^{-1}
m_{CO}	mass flow rate CO at anode feed, kg s^{-1}
m_{CO_2}	mass flow rate CO_2 at anode feed, kg s^{-1}
m_{CH_4}	mass flow rate CH_4 at anode feed, kg s^{-1}
n_{CO}	molar flow rate CO at anode feed, kgmol s^{-1}
n_{CO_2}	molar flow rate CO_2 at anode feed, kgmol s^{-1}
$n_{\text{H}_2\text{O}}$	molar flow rate H_2O at anode feed, kgmol s^{-1}
n_{H_2}	molar flow rate H_2 at anode feed, kgmol s^{-1}
n_{CH_4}	molar flow rate CH_4 at anode feed, kgmol s^{-1}
n_{O_2}	molar flow rate O_2 at anode feed, kgmol s^{-1}
n_{N_2}	molar flow rate N_2 at anode feed, kgmol s^{-1}
n_c	weighted average number of carbon atoms per hydrocarbon molecule in diesel feed
n_e	number of electrons
n_h	theoretical number of moles of hydrogen produced per mol of hydrocarbon
n_{cells}	number of cells in SOFC stack
O_2 to C	oxygen to carbon ratio
p	partial pressure, atm
P	total pressure, atm
Q	heat, kW
S to C	steam to carbon ratio
t	Thickness
T	temperature, K
U_f	fuel utilization in SOFC
U_a	air utilization in SOFC
W	power, kW
X	mole fraction

Greek symbols

ϵ	extent of reaction, kmol s^{-1}
γ	pre-exponential factor
Ω	resistance, ohm

Subscripts

<i>a</i>	anode
<i>c</i>	cathode
COMB	combustion
<i>e</i>	electrons
eff	effective
elec	electric
<i>ij</i>	component (e.g. CO, CO ₂ , H ₂)
<i>k</i>	total number of components
<i>p</i>	constant pressure
ref	reference
rxn	reaction
SOFC	SOFC
SYS	system
WGS	water-gas shift

Superscripts

in	input
out	output
<i>o</i>	initial value

References

- [1] S. Basu, Recent Trends in Fuel Cell Science and Technology, Springer, New York, 2007, ISBN 0387355375.
- [2] E. Baur, H. Preis, Zeitschrift für Elektrochemie und angewandte physikalische Chemie 43 (1937) 727.
- [3] S.C. Singhal, K. Kendall, High Temperature Solid Oxide Fuel Cells: Fundamentals, Design, and Applications, Elsevier, 2003, ISBN 1856173879.
- [4] G. Kolb, Fuel Processing: For Fuel Cells, Wiley-VCH, Weinheim, 2008, ISBN 3527315810.
- [5] J.J. Spivey, D. Shekhawat, D.A. Berry, Fuel Cells: Technologies for Fuel Processing, Elsevier, 2011, ISBN 0444535632.
- [6] NEB, Energy Use in Canada's North: an Overview of Yukon, Northwest Territories, and Nunavut – Energy Facts (2011). Retrieved May 2012 from: <http://www.neb-one.gc.ca>.
- [7] J. Amphlett, R. Mann, B. Peppley, P. Roberge, A. Rodrigues, J. Salvador, Journal of Power Sources 71 (1998) 179–184.
- [8] T.S. Lee, J. Chung, Y.C. Chen, Energy Conversion and Management 52 (2011) 3214–3226.
- [9] K. Kattke, R. Braun, Journal of Power Sources 196 (2011) 6347–6355.
- [10] J. Lawrence, M. Boltze, Journal of Power Sources 154 (2006) 479–488.
- [11] G. Vourliotakis, G. Skevis, M. Founti, International Journal of Hydrogen Energy 36 (2011) 6112–6122.
- [12] F. Baratto, U.M. Diwekar, D. Manca, Journal of Power Sources 139 (2005) 205–213.
- [13] I. Kang, Y. Kang, S. Yoon, G. Bae, J. Bae, International Journal of Hydrogen Energy 33 (2008) 6298–6307.
- [14] M.T. Çoban, C. Ezgi, Journal of Naval Science and Engineering 6 (2010) 59–78.
- [15] O. van Rheinberg, K. Lucka, H. Kohne, T. Schade, J.T. Andersson, Fuel 87 (2008) 2988–2996.
- [16] P. Costamagna, A. Selimovic, M. Del Borghi, G. Agnew, Chemical Engineering Journal 102 (2004) 61–69.
- [17] R.K. Shah, D.P. Sekulić, Fundamentals of Heat Exchanger Design, John Wiley & Sons, New Jersey, 2003, ISBN 0471321710.
- [18] I. EG&G Technical Services, Fuel Cell Handbook, seventh ed., DOE, Morgantown, 2004, ISBN 0899344283.
- [19] L.J.M.J. Blomen, M.N. Mugerwa, Fuel Cell Systems, Springer, New York, 1993, ISBN 0306441586.
- [20] R.D. Parmar, A. Kundu, C. Thurgood, B.A. Peppley, K. Karan, Fuel 89 (2010) 1212–1220.
- [21] J. Larminie, A. Dicks, Fuel Cell Systems Explained, second ed., John Wiley & Sons, West Sussex, 2003, ISBN 978-0-470-84857-9.
- [22] D. Hamby, Health Physics 68 (1995) 195–204.
- [23] D. Hamby, Environmental Monitoring and Assessment 32 (1994) 135–154.
- [24] S. Shaffer, in: Development Update on Delphi's Solid Oxide Fuel Cell Systems, Presented at 2007 SECA Annual Review Meeting (2007). Retrieved from: http://www.netl.doe.gov/publications/proceedings/07/SECA_Workshop/.
- [25] G. Wang, Y. Yang, H. Zhang, W. Xia, Journal of Power Sources 167 (2007) 398–405.